Available online at www.sciencedirect.com
ScienceDirect
Trans. Nonferrous Met. Soc. China 30(2020) 2200−2206
Transactions of Nonferrous Metals Society of China
www.tnmsc.cn

Synthesis and electrochemical performance of V_2O_5/NaV_6O_{15} nanocomposites as cathode materials for sodium-ion batteries

Mu-lan QIN, Wan-min LIU, Yuan-jin XIANG, Wei-gang WANG, Bin SHEN

Hunan Provincial Key Laboratory of Environmental Catalysis & Waste Recycling,
College of Materials and Chemical Engineering, Hunan Institute of Engineering, Xiangtan 411104, China

Received 29 December 2019; accepted 24 June 2020

Abstract: V_2O_5/NaV_6O_{15} nanocomposites were synthesized by a facile hydrothermal method using VO_2(B) nanoarrays as the precursor. X-ray diffraction, scanning electron microscopy and transmission electron microscopy, and galvanostatic charge−discharge test were used to evaluate the structures, morphologies and electrochemical performance of samples, respectively. The results show that the nanocomposites are composed of one-dimensional nanobelts, preserving the morphology of the precursor well, and the hydrothermal reaction time has a significant effect on the phase contents and electrochemical performance of the composites. Compared with pure V_2O_5, V_2O_5/NaV_6O_{15} nanocomposites exhibit enhanced electrochemical performance as cathode for sodium-ion batteries. It should be ascribed to the synergistic effect between V_2O_5 with high capacity and NaV_6O_{15} with good cycling performance, and the introduced massive interfacial areas which can provide additional ion storage sites and improve the electronic and ionic conductivities.

Key words: V_2O_5/NaV_6O_{15}; nanocomposite; cathode material; sodium-ion battery

1 Introduction

Lithium-ion batteries (LIBs) have been widely used in portable electronic products and electric vehicles (EVs) due to their long cycle life and high energy and power densities. However, the limited global reserves of lithium lead to high cost and will seriously hinder the large-scale application of LIBs. Compared with LIBs, sodium-ion batteries (SIBs) have many potential advantages such as abundant sodium resources and low cost, which are suitable for large-scale storage [1−5]. However, the large ionic size (1.02 Å) and low standard electrochemical potential (2.71 V) of Na result in low reversible specific capacity and energy density, hindering further developments of SIBs [6,7]. Thus, developing cathode materials with high capacity for SIBs is an urgent requirement [8].

Vanadium pentoxide (V_2O_5), which has been widely studied as a cathode material for LIBs [9−14], shows great potential for SIBs owing to its high theoretical capacity (294 mA·h/g for 2 Na ions intercalation) [15]. However, due to larger radius of Na^+, the intercalation of Na^+ in V_2O_5 is more difficult, and V_2O_5 suffers from poor electronic and ionic conductivities, thus resulting in lower reversible capacity and worse rate capability [16−19]. To resolve these issues, one of the most effective strategies is to design nanostructured V_2O_5, such as nanobelts [20], nanospheres [21] and nanosheets [22], which could decrease the transport pathways for sodium ions and enhance the contact area between the active material and electrolyte. On the other hand, NaV_6O_{15} exhibits much stable cycling performance when used as a cathode for SIBs [23−26], although it has relatively low discharge capacity. So, V_2O_5/

Foundation item: Project (2020JJ5102) supported by the Natural Science Foundation of Hunan Province, China; Project (19A111) supported by the Scientific Research Fund of Hunan Provincial Education Department, China
Corresponding author: Wan-min LIU; Tel: +86-13787101796; E-mail: william@hnie.edu.cn
DOI: 10.1016/S1003-6326(20)65372-9

NaV_6O_{15} composites with nanostructures should have good electrochemical performance as cathode for SIBs for the synergistic effect between V_2O_5 and NaV_6O_{15}. NIU et al [27] reported that three-dimensional V_2O_5/NaV_6O_{15} hierarchical hetero-structure microspheres show better electrochemical performance than pure V_2O_5 as cathode for LIBs [27]. However, there seems to be less report about V_2O_5/NaV_6O_{15} nanocomposites as cathode for SIBs.

Herein, a hydrothermal method was introduced to synthesize V_2O_5/NaV_6O_{15} nanocomposites using VO_2(B) nanoarrays as the precursor, and the electrochemical properties of V_2O_5/NaV_6O_{15} nanocomposites as cathode materials for SIBs were investigated.

2 Experimental

2.1 Synthesis of V_2O_5/NaV_6O_{15} nanocomposites

All the reagents and solvent were of analytical grade and used without further purification. Firstly, VO_2(B) precursor with a thickness of 10−20 nm was synthesized according to a hydrothermal method reported in our previous work [28]. 0.5 g V_2O_5 powder was added with 20 mL distilled water and 10 mL ethyleneglycol (EG), which was then maintained at 180 °C for 18 h to obtain the VO_2(B) precursor. Secondly, 6 mmol VO_2(B) was added into 15 mL NaOH solution with concentration of 0.1 mol/L, which was then sealed in Teflon-lined stainless steel autoclaves and maintained at 180 °C for different durations of 2, 6 and 12 h. After being cooled down to room temperature, the precipitate was filtered off, washed with distilled water several times and then dried at 80 °C overnight. Finally, the collected powder was calcined at 350 °C for 4 h in air to obtain the composites. For comparison, pure V_2O_5 was synthesized by calcining VO_2(B) precursor at 350 °C for 4 h in air.

2.2 Characterization

The phase structures of obtained products were determined by X-ray diffraction (XRD) (Rigaku D/max2500 XRD with Cu K_α radiation, λ=1.54178 Å). A scanning electron microscope (SEM) (FEI Sirion200) and a field emission transmission electron microscope (FETEM) (JEOL JEM−2100F) were used to characterize the morphologies of obtained products.

The V_2O_5/NaV_6O_{15} nanocomposites were assembled into coin-type cells to evaluate their electrochemical properties. V_2O_5/NaV_6O_{15} nano-composites, acetylene black and polyvinylidene-fluoride (PVDF) binder in a mass ratio of 7:2:1 were dispersed in *N*-methyl-2-pyrrolidone (NMP) solution to make the slurry, which was then coated on an aluminum foil and dried in a vacuum oven at 120 °C for 12 h to make the cathode electrode. Coin-type cells (CR 2025) were assembled using glass fiber (Whitman GF/C) as the separator and 1.0 mol/L $NaClO_4$ dissolved in ethylene carbonate (EC)-diethyl carbonate (DEC) (1:1 in volume) as the electrolyte. The galvanostatic charge/discharge characteristics of the cells were recorded with a Land battery tester (Land CT2001A), and the electrochemical workstation (Multi Autolab M204, Metrohm) was applied to acquiring CV curves.

3 Results and discussion

The XRD patterns of V_2O_5/NaV_6O_{15} composites obtained with different reaction time and the standard V_2O_5 and NaV_6O_{15} patterns are shown in Fig. 1. It can be seen that the composites obtained with the hydrothermal reaction time of 2, 6 and 12 h, respectively, are composed of orthorhombic V_2O_5 phase and monoclinic NaV_6O_{15} phase, with no evidence of other impurity phases, which indicates that V_2O_5/NaV_6O_{15} composites can be easily synthesized within 2 h. Moreover, the sharp peaks in the patterns indicate that the composites are well crystallized.

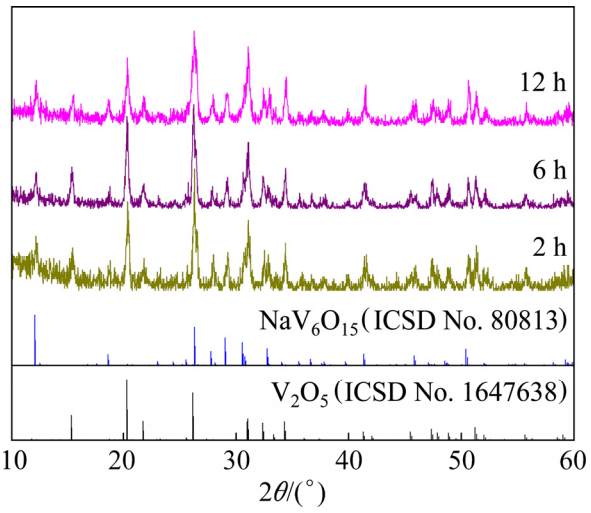

Fig. 1 XRD patterns of V_2O_5/NaV_6O_{15} composites obtained with different hydrothermal reaction time

The Rietveld refinement method (Jade 9.0 software, MDI, USA) was used to refine the XRD pattern of V_2O_5/NaV_6O_{15} composites obtained with the hydrothermal reaction time of 6 h to analyze the crystal structures and phases. As shown in Fig. 2, all the diffraction peaks can be well indexed to orthorhombic V_2O_5 phase [space group: *Pmmn* (59), ICSD No. 1647638] and monoclinic layered NaV_6O_{15} phase [space group: *C*2/*m* (12), ICSD No. 80813], and no other impurity phase is detected. Table 1 gives the refined cell parameters of V_2O_5 and NaV_6O_{15} in V_2O_5/NaV_6O_{15} composites. The observed and calculated patterns match well, and the reasonably small *R* factor (8.47%) suggests that the refinement results are convincible. The parameters of V_2O_5 and NaV_6O_{15} present little distortion in V_2O_5/NaV_6O_{15} composites compared with the pure individual phase, and the phase contents of V_2O_5 and NaV_6O_{15} are 69 and 31 wt.%, respectively. By prolonging the hydrothermal reaction time to 12 h, the phase contents of V_2O_5 and NaV_6O_{15} change to 40 and 60 wt.%, respectively, indicating that hydrothermal reaction time has a significant effect on the phase contents.

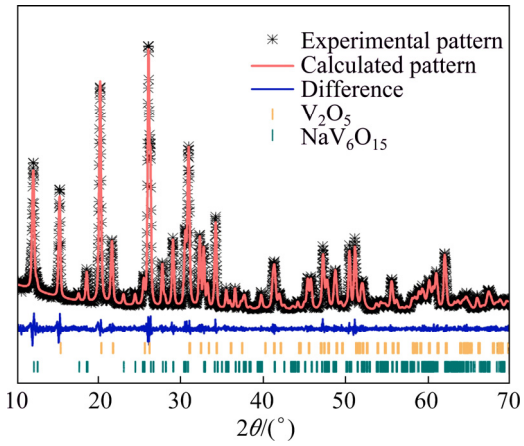

Fig. 2 XRD pattern with Rietveld refinement of V_2O_5/NaV_6O_{15} composite obtained with hydrothermal reaction time of 6 h

The morphologies of V_2O_5/NaV_6O_{15} composites obtained with different hydrothermal reaction time were studied by SEM and the results are shown in Figs. 3(a−c). It can be seen that V_2O_5/NaV_6O_{15} composites obtained with 2, 6 and 12 h, respectively, are composed of one-dimensional nanobelts, preserving the morphology of the precursor well. Figure 3(d) shows the TEM image of V_2O_5/NaV_6O_{15} nanocomposites obtained with the hydrothermal reaction time of 6 h. It is interesting that the composites display interconnected nanosheet structure, which is beneficial to shortening ion diffusion distance and providing large contact area for electrochemical reactions [15]. Moreover, the phase boundaries of V_2O_5 and NaV_6O_{15} phases of V_2O_5/NaV_6O_{15} nanocomposites and uniform distribution of elements Na, V and O can be detected by HRTEM and SEM−EDS mapping, respectively, as shown in earlier work [29]. The existence of substantial phase boundaries may introduce numerous crystal defects and active sites [30], which will promote the ion conductivity as well as supply vacancy for Na^+ insertion.

Figure 4(a) shows the discharge−charge curves of the first cycles of V_2O_5/NaV_6O_{15} nanocomposites obtained with different hydrothermal reaction time within the voltage range of 1.5−3.8 V at 20 mA/g. Three discharge plateaus located around 2.7, 2.2 and 2.0 V can be identified as the insertion of Na^+ into V_2O_5/NaV_6O_{15} nanocomposites. The multiple plateaus indicate multiple steps of sodium ions intercalation process [23,31]. In addition, high initial specific discharge capacities of 184, 209 and 133 mA·h/g are obtained for V_2O_5/NaV_6O_{15} nanocomposites obtained with 2, 6 and 12 h, respectively. However, for pure V_2O_5, only two discharge plateaus located around 2.1 and 1.9 V and an initial specific discharge capacity of 110 mA·h/g are observed.

Table 1 Refined unit cell lattice parameters of V_2O_5 and NaV_6O_{15} in V_2O_5/NaV_6O_{15} composites and standard data of V_2O_5 (ICSD No. 1647638) and NaV_6O_{15} (ICSD No. 80813)

Sample	Lattice parameters					Phase content/wt.%	*R*/%
	a/nm	*b*/nm	*c*/nm	*β*/(°)	*V*/nm^3		
V_2O_5 in composites	1.15216	0.35675	0.3766	90.0000	0.1798	68.675	8.47
V_2O_5	1.15100	0.35630	0.43690	90.0000	0.1792	–	–
NaV_6O_{15} in composites	1.00922	0.36116	1.54070	109.524	0.5293	31.325	8.47
NaV_6O_{15}	1.00883	0.36172	1.54493	109.572	0.5311	–	–

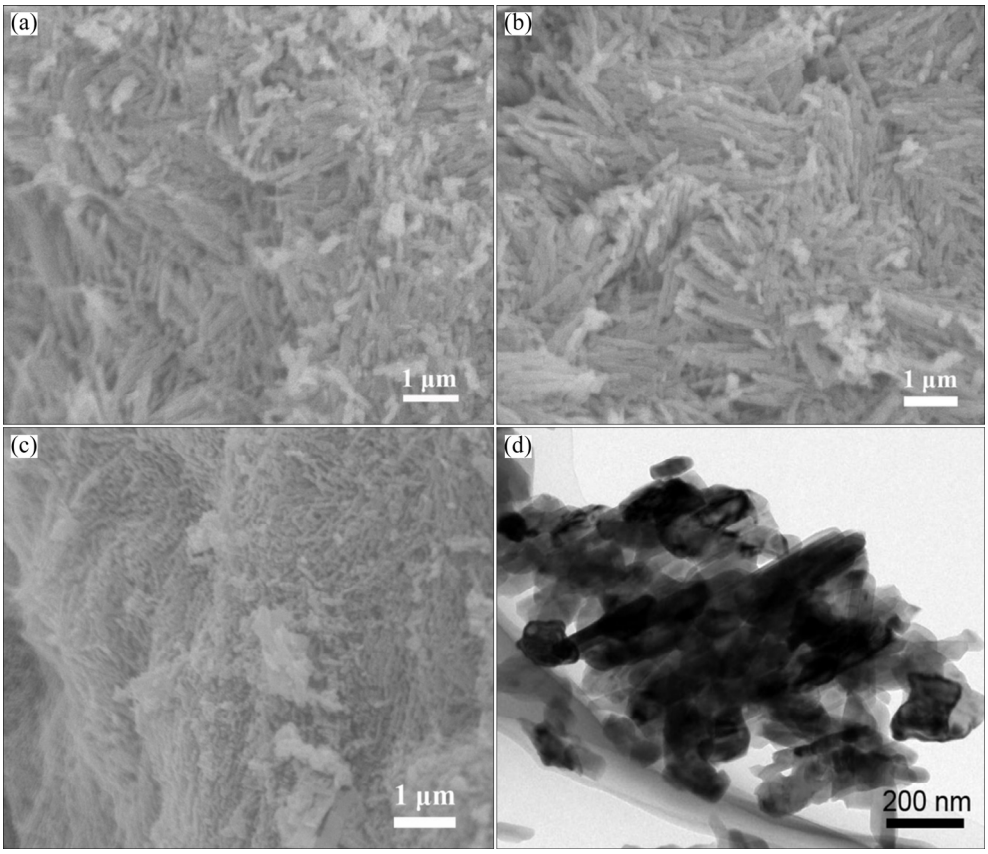

Fig. 3 SEM images of V_2O_5/NaV_6O_{15} nanocomposites obtained with hydrothermal reaction time of 2 h (a), 6 h (b) and 12 h (c), and TEM image of V_2O_5/NaV_6O_{15} nanocomposite obtained with hydrothermal reaction time of 6 h (d)

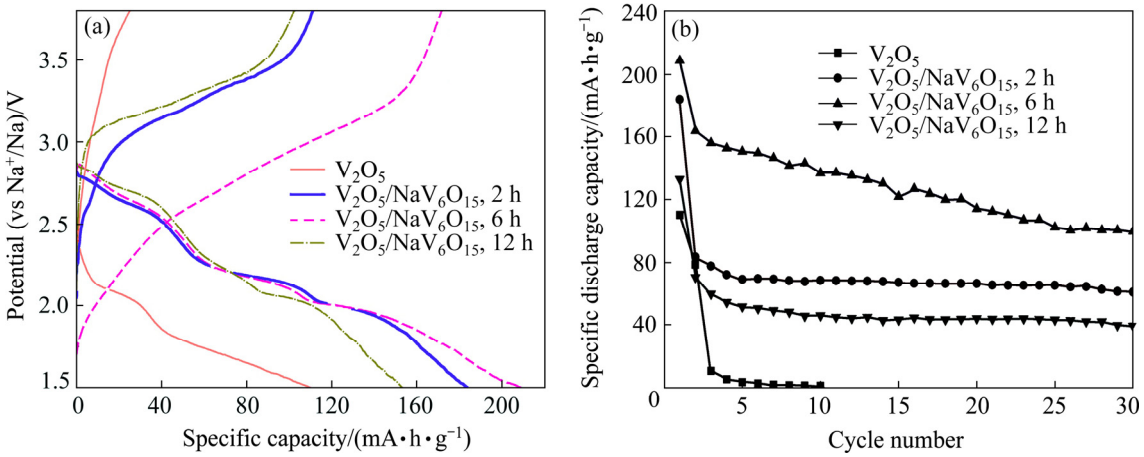

Fig. 4 Galvanostatic discharge–charge curves (a) and cycling performance (b) of V_2O_5/NaV_6O_{15} nanocomposites and pure V_2O_5 in voltage range of 1.5−3.8 V at current density of 20 mA/g

Figure 4(b) compares the cyclic performance of V_2O_5/NaV_6O_{15} nanocomposites obtained with different hydrothermal reaction time at 20 mA/g. At the second cycle, V_2O_5/NaV_6O_{15} nanocomposites obtained with 6 h deliver a specific discharge capacity of 164 mA·h/g and its capacity retains to be 100 mA·h/g after 30 cycles. V_2O_5/NaV_6O_{15} nanocomposites obtained with 2 and 12 h deliver much lower discharge capacities of 84 and 70 mA·h/g at the second cycle, and the capacities then drop to 61 and 40 mA·h/g after 30 cycles, respectively. These results indicate that the hydrothermal reaction time has a significant effect on the electrochemical performance of V_2O_5/NaV_6O_{15} nanocomposites by affecting the phase contents of the nanocomposites. While for pure

V_2O_5, the capacity can be nearly ignored after 10 cycles, just be 1 mA·h/g. Compared with pure V_2O_5, V_2O_5/NaV_6O_{15} nanocomposites show enhanced electrochemical performance, which should be ascribed to the construction of nanocomposites. On one hand, the synergistic effect in V_2O_5/NaV_6O_{15} nanocomposites is favorable to inherit the high capacity of V_2O_5 and good cycling performance of NaV_6O_{15} [29,32]. On the other hand, introducing nanocomposites will increase massive interfacial areas, which can provide additional ion storage sites and improve the electronic and ionic conductivities [33,34]. In addition, there is obvious capacity fading in initial cycles, which could be mainly due to the generation of solid electrolyte interphase (SEI) formed by the electrolyte decomposition [21,35].

Figure 5 presents the cyclic voltammetry (CV) curves of V_2O_5/NaV_6O_{15} nanocomposites obtained with the hydrothermal reaction time of 6 h at a scan rate of 0.1 mV/s in the voltage range of 1.5−4.0 V. During the first reduction process, three obvious cathodic peaks at 2.7, 2.0 and 1.7 V are observed, which can be attributed to the multi-step insertion of Na^+ ions into V_2O_5/NaV_6O_{15} nanocomposites. For the corresponding oxidation process, two anodic peaks are observed at 3.1 and 3.6 V, indicating the multi-step Na^+ ions extraction processes. The first CV curve possesses some difference compared with the latter ones, and this phenomenon should be ascribed to the structure rearrangement of the composites after Na^+ ion insertion in the first cycle [15,23]. With the increase of cycle number, the CV curves are almost equal in size, suggesting a high reversibility of the insertion/extraction reactions.

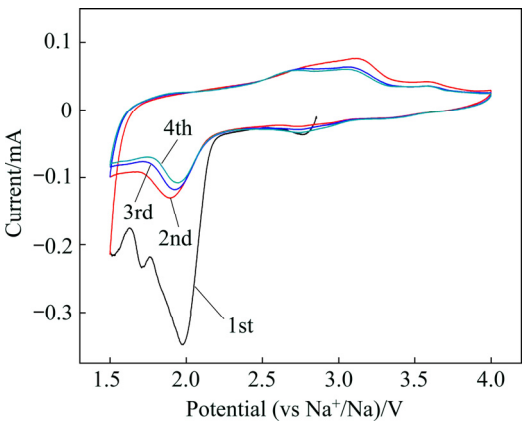

Fig. 5 CV curves of V_2O_5/NaV_6O_{15} nanocomposites at scan rate of 0.1 mV/s

The second discharge−charge curves of V_2O_5/NaV_6O_{15} nanocomposites obtained with 6 h in the voltage range of 1.5−4.0 V at different current densities are shown in Fig. 6(a). The charge−discharge plateaus correspond well with the peak positions shown on the CV curves (Fig. 5), and the capacities of 176, 126 and 101 mA·h/g are obtained at 20, 50 and 100 mA/g, respectively. Figure 6(b) shows the cycling performance of V_2O_5/NaV_6O_{15} nanocomposites at different current densities. Initial specific discharge capacities of 231, 201 and 173 mA·h/g are obtained at current densities of 20, 50 and 100 mA/g, respectively. The capacities decrease to 101, 93 and 70 mA·h/g after 50 cycles, with the retention of 57.4%, 73.8% and 69.3% of capacities at the second cycle, respectively. It can be seen from Figs. 5 and 6 that the composites show higher capacity and better cycling performance in the voltage range of 1.5−4.0 V, which indicates that the voltage range has a significant effect on the electrochemical properties of V_2O_5/NaV_6O_{15} nanocomposites. The synthesized nanocomposites

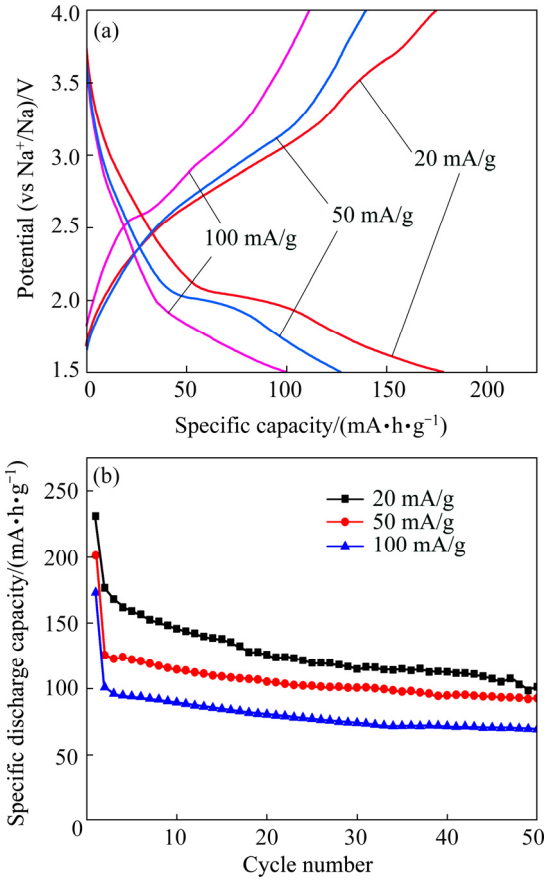

Fig. 6 Galvanostatic discharge–charge curves (a) and cycling performance (b) of V_2O_5/NaV_6O_{15} nanocomposites in voltage range of 1.5−4.0 V at different current densities

in this work display better electrochemical performance compared with the pure V_2O_5 and NaV_6O_{15} reported in earlier literatures [24,31], which can be ascribed to the construction of nanocomposites.

4 Conclusions

(1) V_2O_5/NaV_6O_{15} nanocomposites were synthesized successfully by a hydrothermal method. The hydrothermal reaction time has a significant effect on the electrochemical performance of the composites by affecting the phase contents.

(2) V_2O_5/NaV_6O_{15} nanocomposites show enhanced electrochemical performance compared with pure V_2O_5, which should be attributed to the synergistic effect between V_2O_5 and NaV_6O_{15}, and the introduced massive interfacial areas.

(3) V_2O_5/NaV_6O_{15} nanocomposites deliver a high initial discharge capacity of 231 mA·h/g in the voltage range of 1.5−4.0 V, which indicates that V_2O_5/NaV_6O_{15} nanocomposites are potential cathode materials for sodium-ion batteries.

References

[1] KUNDU D, TALAIE E, DUFFORT V, NAZAR L F. The emerging chemistry of sodium ion batteries for electrochemical energy storage [J]. Angewandte Chemie, 2015, 54(11): 3431−3448.

[2] KIM S W, SEO D H, MA X, CEDER G, KANG K. Electrode materials for rechargeable sodium-ion batteries: Potential alternatives to current lithium-ion batteries [J]. Advanced Energy Materials, 2012, 2(7): 710−721.

[3] LIANG Shu-quan, CHENG Yi-bing, FANG Guo-zhao, CAO Xin-xin, SHEN Wen-jian, ZHONG Jie, PAN An-qiang, ZHOU Jiang. Research progress of key materials for energy photoelectric conversion and large-scale energy storage secondary batteries [J]. The Chinese Journal of Nonferrous Metals, 2019, 29(9): 2064−2114. (in Chinese)

[4] XU Bao-lin, QI Shi-han, HE Peng-bin, MA Jian-min. Antimony- and bismuth-based chalcogenides for sodium-ion batteries [J]. Chemistry−An Asian Journal, 2019, 14(17): 2925−2937.

[5] QI Shi-han, XU Bao-lin, TIONG V T, HU Jin, MA Jian-min. Progress on iron oxides and chalcogenides as anodes for sodium-ion batteries [J]. Chemical Engineering Journal, 2020, 379: 122261.

[6] KIM H, KIM H, DING Z, LEE M H, LIM K, YOON G, KANG K. Recent progress in electrode materials for sodium-ion batteries [J]. Advanced Energy Materials, 2016, 6(19): 1600943.

[7] YAN Zhan-heng, YANG Qin-Wen, WANG Qing-hong, MA Jian-min. Nitrogen doped porous carbon as excellent dual anodes for Li- and Na-ion batteries [J]. Chinese Chemical Letters, 2020, 31(2): 583−588.

[8] CHEN Ren-jie, LUO Rui, HUANG Yong-xin, WU Feng, LI Li. Advanced high energy density secondary batteries with multi-electron reaction materials [J]. Advanced Science, 2016, 3(10): 1600051.

[9] WU Chang-zheng, FENG Feng, XIE Yi. Design of vanadium oxide structures with controllable electrical properties for energy applications [J]. Chemical Society Reviews, 2013, 42(12): 5157−5183.

[10] WANG Ying, CAO Guo-zhong. Synthesis and enhanced intercalation properties of nanostructured vanadium oxides [J]. Chemistry of Materials, 2006, 18(12): 2787−2804.

[11] CHERNOVA N A, ROPPOLO M, DILLON A C, WHITTINGHAM M S. Layered vanadium and molybdenum oxides: Batteries and electrochromics [J]. Journal of Materials Chemistry, 2009, 19(17): 2526−2552.

[12] WU Chang-zheng, XIE Yi. Promising vanadium oxide and hydroxide nanostructures: From energy storage to energy saving [J]. Energy & Environmental Science, 2010, 3(9): 1191−1206.

[13] MAI Li-qiang, XU Xu, XU Lin, HAN Chun-hua, LUO Yan-zhu. Vanadium oxide nanowires for Li-ion batteries [J]. Journal of Materials Research, 2011, 26(17): 2175−2185.

[14] CHEN Peng-yu, ZHENG Guo-tao, TANG Jie, LI Song, WEN Zhong-sheng, JI Shi-jun, SUN Jun-cai. Recent progress of three-dimensional hierarchical structure V_2O_5 Li ion cathode materials [J]. The Chinese Journal of Nonferrous Metals, 2019, 29(1): 100−114. (in Chinese)

[15] WANG Hong-kuan, GAO Xue-ping, FENG Jin-kui, XIONG Sheng-lin. Nanostructured V_2O_5 arrays on metal substrate as binder free cathode materials for sodium-ion batteries [J]. Electrochimica Acta, 2015, 182: 769−774.

[16] RAJU V, RAINS J, GATES C, LUO W, WANG X, STICKLE W F, STUCKY G D, JI X. Superior cathode of sodium-ion batteries: Orthorhombic V_2O_5 nanoparticles generated in nanoporous carbon by ambient hydrolysis deposition [J]. Nano Letters, 2014, 14(7): 4119−4124.

[17] CHEN Jiu-cun, LI Wen-jun, JIANG Jian, WU Chao, LIU Yin-qin. Facile and creative design of hierarchical vanadium oxides@graphene nanosheet patterns [J]. RSC Advances, 2016, 6(16): 13323−13327.

[18] UCHAKER E, ZHENG Y Z, LI S, CANDELARIA S L, HU S, CAO G Z. Better than crystalline: Amorphous vanadium oxide for sodium-ion batteries [J]. Journal of Materials Chemistry A, 2014, 2(43): 18208−18214.

[19] ALI G, LEE J H, OH S H, CHO B W, NAM K W, CHUNG K Y. Investigation of the Na intercalation mechanism into nanosized V_2O_5/C composite cathode material for Na-ion batteries [J]. ACS Applied Materials & Interfaces, 2016, 8(9): 6032−6039.

[20] SU Da-wei, WANG Guo-xiu. Single-crystalline bilayered V_2O_5 nanobelts for high-capacity sodium-ion batteries [J]. ACS Nano, 2013, 7(12): 11218−11226.

[21] SU D W, DOU S X, WANG G X. Hierarchical orthorhombic V_2O_5 hollow nanospheres as high performance cathode materials for sodium-ion batteries [J]. Journal of Materials Chemistry A, 2014, 2(29): 11185−11194.

[22] ZHU Kai, ZHANG Chao-feng, GUO Shao-hua, YU Hai-jun, LIAO Kai-ming, CHEN Gang, WEI Ying-jin, ZHOU

Hao-shen. Sponge-like cathode material self-assembled from two-dimensional V_2O_5 nanosheets for sodium-ion batteries [J]. ChemElectroChem, 2015, 2(11): 1660−1664.

[23] HE Han-an, ZENG Xian-guang, WANG Hai-yan, CHEN Na, SUN Dan, TANG You-gen, HUANG Xiao-bing, PAN Ying-fen. NaV_6O_{15} nanoflakes with good cycling stability as a cathode for sodium ion battery [J]. Journal of The Electrochemical Society, 2015, 162(1): A39−A43.

[24] JIANG Dan-lu, WANG Hui, LI Guo-peng, LI Guang-qiang, LAN Xin-zheng, ABIB M H, ZHANG Zhong-ping, JIANG Yang. Self-combustion synthesis and ion diffusion performance of NaV_6O_{15} nanoplates as cathode materials for sodium-ion batteries [J]. Journal of the Electrochemical Society, 2015, 162(4): A697−A703.

[25] SHANG Chao-qun, HU Le, LIN Qin, FU Xue-lian, WANG Xin, ZHOU Guo-fu. Integration of $NaV_6O_{15}{\cdot}nH_2O$ nanowires and rGO as cathode materials for efficient sodium storage [J]. Applied Surface Science, 2019, 494: 458−464.

[26] DONG Yi-fan, XU Jun-ling, CHEN Meng-yu, GUO Yu-mei, ZHOU Guo-dong, LI Nan, ZHOU Shuang, WONG Ching-ping. Self-assembled NaV_6O_{15} flower-like microstructures for high-capacity and long-life sodium-ion battery cathode [J]. Nano Energy, 2020, 68: 104357.

[27] NIU Chao-jiang, LIU Xiong, MENG Jia-shen, XU Lin, YAN Meng-yu, WANG Xuan-peng, ZHANG Guo-bin, LIU Ziang, XU Xiao-ming, MAI Li-qiang. Three dimensional V_2O_5/NaV_6O_{15} hierarchical heterostructures: Controlled synthesis and synergistic effect investigated by in situ X-ray diffraction [J]. Nano Energy, 2016, 27:147−156.

[28] QIN Mu-lan, LIANG Qiang, PAN An-qiang, LIANG Shu-quan, ZHANG Qing, TANG Yan, TAN Xiao-ping. Template-free synthesis of vanadium oxides nanobelt arrays as high-rate cathode materials for lithium ion batteries [J]. Journal of Power Sources, 2014, 268: 700−705.

[29] QIN Mu-lan, LIU Wan-min, SHAN Lu-tong, FANG Guo-zhao, CAO Xin-xin, LIANG Shu-quan, ZHOU Jiang. Construction of V_2O_5/NaV_6O_{15} biphase composites as aqueous zinc-ion battery cathode [J]. Journal of Electroanalytical Chemistry, 2019, 847: 113246.

[30] FANG Guo-zhao, WU Zhuo-xi, ZHOU Jiang, ZHU Chu-yu, CAO Xin-xin, LIN Tian-quan, CHEN Yu-ming, WANG Chao, PAN An-qiang, LIANG Shu-quan. Observation of pseudocapacitive effect and fast ion diffusion in bimetallic sulfides as an advanced sodium-ion battery anode [J]. Advanced Energy Materials, 2018, 8: 1703155.

[31] NGHIA N V, LONG P D, TAN T A, JAFIAN S, HUNG I M. Electrochemical performance of a V_2O_5 cathode for a sodium ion battery [J]. Journal of Electronic Materials, 2017, 46(6): 3689−3694.

[32] FANG Guo-zhao, WANG Qi-chen, ZHOU Jiang, LEI Yong-peng, CHEN Zi-xian, WANG Zi-qing, PAN An-qiang, LIANG Shu-quan. Metal organic framework-templated synthesis of bimetallic selenides with rich phase boundaries for sodium-ion storage and oxygen evolution reaction [J]. ACS Nano, 2019, 13: 5635−5645.

[33] WU Qi-li, XU Jun-gu, YANG Xian-feng, LU Feng-qi, HE Shi-man, YANG Jing-ling, FAN Hong Jin, WU Ming-mei. Ultrathin anatase TiO_2 nanosheets embedded with TiO_2−B nanodomains for lithium-ion storage: Capacity enhancement by phase boundaries [J]. Advanced Energy Materials, 2015, 5: 1401756.

[34] MAGASINSKI A, DIXON P, HERTZBERG B, KVIT A, AYALA J, YUSHIN G. High-performance lithium-ion anodes using a hierarchical bottom-up approach [J]. Nature Materials, 2010, 9: 353−358.

[35] SU Da-wei, DOU Shi-xue, WANG Guo-xiu. Hierarchical vanadium pentoxide spheres as high-performance anode materials for sodium-ion batteries [J]. ChemSusChem, 2015, 8(17): 2877−2882.

钠离子电池正极用 V_2O_5/NaV_6O_{15} 纳米复合材料的制备与电化学性能

秦牡兰，刘万民，向垣锦，王伟刚，申 斌

湖南工程学院 材料与化工学院 环境催化与废弃物再生化湖南省重点实验室，湘潭 411104

摘 要：采用 VO_2(B)纳米阵列作为前驱体，通过水热法制备 V_2O_5/NaV_6O_{15} 纳米复合材料。通过 X 射线衍射、扫描电镜、透射电镜和恒流充放电测试对材料的结构、形貌和电化学性能进行表征。结果表明，纳米复合材料由一维纳米带组成，较好地保留了前驱体的形貌；水热反应时间对材料的相组成和电化学性能有显著的影响。V_2O_5/NaV_6O_{15} 纳米复合材料比纯 V_2O_5 显示出更好的电化学性能，这归因于 V_2O_5/NaV_6O_{15} 纳米复合材料中具有高容量的 V_2O_5 和高循环稳定性的 NaV_6O_{15} 之间的协同效应，以及纳米复合材料中引入的大量相界面为钠离子嵌入提供了额外的位点并促进电子和离子的传输。

关键词：V_2O_5/NaV_6O_{15}；纳米复合材料；正极材料；钠离子电池

(Edited by Bing YANG)